Research

Vibrational resonances in driven oscillators with position-dependent mass

T. O. Roy-Layinde[1], U. E. Vincent[2,3],
S. A. Abolade[4], O. O. Popoola[4],
J. A. Laoye[1] and P. V. E. McClintock[3]

[1]Department of Physics, Olabisi Onabanjo University, Ago-Iwoye, Ogun State, Nigeria
[2]Department of Physical Sciences, Redeemer's University, P.M.B. 230, Ede, Nigeria
[3]Department of Physics, Lancaster University, Lancaster LA1 4YB, United Kingdom
[4]Department of Physics, University of Ibadan, Nigeria

The vibrational resonance (VR) phenomenon has received a great deal of research attention over the two decades since its introduction. The wide range of theoretical and experimental results obtained has, however, been confined to VR in systems with constant mass. We now extend the VR formalism to encompass systems with position-dependent mass (PDM). We consider a generalized classical counterpart of the quantum mechanical nonlinear oscillator with PDM. By developing a theoretical framework for determining the response amplitude of PDM systems, we examine and analyse their VR phenomenona, obtain conditions for the occurrence of resonances, show that the role played by PDM can be both inductive and contributory, and suggest that PDM effects could usefully be explored to maximise the efficiency of devices being operated in VR modes. Our analysis suggests new directions for the investigation of VR in a general class of PDM systems.

1. Introduction

Nonlinear science has attracted global interest on account of its broad applications to a diversity of disciplines. These range from the physical to the technological fields, and from biology to medicine, as well as the social sciences [1]. It describes the dynamics of systems defined by nonlinear functions. Although the behaviour of such

nonlinear systems is typically controlled by quite simple deterministic or stochastic laws, their dynamics can nonetheless be highly complicated and often counter-intuitive. The nonlinearity inherent in most systems, particularly in experimental situations, may appear in a diversity of forms, such as physical, structural, frictional, or geometrical and, in many contexts, external forces [2]. A major cause of structural nonlinearity in materials, frequently ignored because of its complex mathematical implications, is that of varying inertial mass. Such changes affect considerably the structural nonlinearity of dynamical systems [2,3].

Varying mass usually implies that the mass is dependent on a generalized coordinate: either velocity, or position or time; or on a function of both position and time. The mass changes with respect to these variables during motion as the result of addition and/or removal of particles [4]. In general, systems with varying masses are encountered in fields such as rocket science, tethered satellite dynamics [3]), meteorites [5], aerology, oceanography [5]), offshore and civil engineering [6]. They are also applicable in condensed matter system such as NH_3 inverted potential structure [7] and semiconductor heterogeneous structures [8,9], particle-accreting systems such as raindrops [10], as well as accretion of planets and asteroids in the early solar system [11]. They can be classified into two main groups: continuous-particle-ejecting systems or discrete-particle-ejecting systems, depending on whether or not the addition/removal of particles to/from the initial bulk mass takes place over an infinitesimally short time [3,4]. In systems with continuous mass variation, the mass-time (or mass-position) function can either be deterministic or stochastic [12]. The dynamics of stochastic systems has been well studied, particularly in systems under the combined influences of a deterministic signal, an added noisy excitation, and a random mass. There have been numerous analyses and applications involving the phenomenon of stochastic resonance [13]. However, in many physical systems, the associated inertial mass is neither constant, nor stochastically varying, nor dynamically changing with time but, rather, is explicitly position-dependent.

In position-dependent mass (PDM) systems, where the variable mass is specified in terms of its position, several types of mass variation function have been considered [14,15]. Much of the works were related to quantum variants [16], but classical PDM systems have also received considerable attention, with an emphasis on derivation of the dynamical equation of motion from Lagrangian or Hamiltonian dynamics [14,17–19]. Notably, the classical equation of motion of PDM systems contains an extra non-conservative generalized force term of quadratic order in the modified Newton's equation, a term which is nonlinear in velocity and linearly proportional to the mass gradient [18–20]. This nonlinearity can impact on the dynamics of the system, including the occurrence of resonance which we demonstrate for the first time below.

Traditionally, resonance occurs in a system when its natural frequency of vibration is equal to the frequency of an external driving force, leading to an enhanced output response [21]. However, the term has been generalized to define more broadly all processes involving the enhancement, suppression or optimization of a system's response through the modulation of any system property, thereby removing the restriction to frequency matching. When the resonance takes place in a nonlinear system it is called nonlinear resonance and, in this case, frequency matching is absent except under special condition [22] and hence is not a prerequisite for the occurrence of resonance.

Nonlinear resonances are characterized by the enhancement of a system's maximum response at low-frequency (LF) induced by an external driving force, and it manifests in diverse forms, depending on the nature of the force [21]. When the force takes the form of a high-frequency (HF) periodic signal, it results in what is now known as *vibrational resonance* (VR) [23,24]: in VR, an optimal amplitude of HF excitation applied to a nonlinear system alters its response to an LF signal in a resonant fashion. The effect of the HF excitation is thus similar to the effect of noise in the better-known phenomenon of *stochastic resonance* (SR) [13,25–27]. Other important forms of nonlinear resonance have been discussed by Rajasekar and Sanjuán [21].

In parallel with SR, VR has also been subjected to close research attention over the last two decades, in large part due to its potential industrial applications. These relate particularly to

communications, for filtering, optimisation and control of signal output, signal identification, separation and extraction of signals, noise attenuation, or for emphasising specific aspects of a signal. Other advanced technological applications include ratchet-like devices such as switches, amplifiers, sensors, transducers, filters, and nonlinear mixers, which offer the prospect of improved operating conditions and efficiency when operated within VR regimes [21].

Following its introduction by Landa and McClintock [23] and motivated by the aforementioned potential applications, VR has now been demonstrated and analyzed in a diversity of model systems both theoretically, numerically and experimentally, cutting across many fields such as neuroscience, plasma physics, laser physics, acoustics and engineering. Specifically, the VR phenomenon has been investigated in bistable systems [24,28–35], multistable systems [36,37], ratchet devices [38], excitable systems [39], quintic oscillators [40–44], coupled oscillators [25,45–47], overdamped systems [30], delayed dynamical systems [44, 46,48–52], asymmetric Duffing oscillators [53], fractional order oscillators [32,42,54], neural models [39,50,55–61], oscillatory networks [46,55,58–60,62–64], biological nonlinear systems [49, 61,64] parametrically excited systems [34,65–69], systems with nonlinear damping [37,70–72], and deformed potential [73], disordered systems [74], quantum systems [75,76], as well as harmonically trapped and roughed potentials [72,77]. More importantly, VR has been demonstrated in experimental realisations, especially in multistable systems, arrays of hard limiters, bistable vertical-cavity surface-emitting lasers [28,29,33,78–81] and Chua circuits [82,83].

Additional novel phenomena, intriguing properties, and new directions for potential applications have been found more recently. For example, a connection between VR and phase-locking modes was established by Morfu and Bordet [84]. Rajamani *et al.* [85] observed a novel ghost-vibrational resonance, while vibrational antiresonance has been reported by Sakar and Shankar Ray [47]. Furthermore, the existence of subharmonic and superharmonic resonances [86] and higher harmonics [87] were also reported. In another line of development, new methods of analysis in which nonlinear systems are driven by aperiodic forces have been investigated – giving birth to fresh perspectives for aperiodic vibrational resonance, re-scaled aperiodic vibrational resonance and twice-sampled aperiodic vibrational resonance methods [88], re-scaled and improved twice-sampling [68], and a new spectral amplification factor approach [89].

The potential applications of VR have been explored in, for instance, improving energy harvesting from mechanical vibrations [90], energy detectors [91], the detection, transmission and amplification of signals [60,92,93], and the detection of faults in bearings [94–97], as well as in the design of Dual Input Multiple Output (DIMO) logic gates and memory devices [83,98–100].

The large and growing body of research on VR has assumed constant mass, and no attempt has been made to examine VR in systems whose mass is spatially varying. Recently, Usama *et al.* [101] examined the role of constant-non-unitary mass for VR in a multistable system [37]. They showed that variation in mass can complement the role of bi-harmonic external forcing much like damping nonlinearity [37,71], and can also determine the condition for resonance. However, only numerical results were presented, without an underpinning theory. Moreover, similarly to previous analyses, the variation in mass was assumed to be position-independent. It is important to emphasize that, when mass variation occurs in natural and mechanical systems, it can be associated with jump-like variations in velocity or angular velocity which, in practical applications, could lead to serious malfunction and/or destruction of parts of the machines in question, as can sometimes occur due to resonances. Thus, the analysis of VR in systems with position-dependent mass is necessary for both scientific and technological purposes.

In this paper, we consider a simple, but general, PDM system with a regular mass function consisting of a constant mass (mass amplitude) and a quadratic spatial nonlinearity, modelled by a bistable potential [14,18,20]. We develop a general theoretical framework for dealing with VR in PDM systems. Theoretical results are complemented with numerical simulations. The rest of the paper is structured as follows. In Section 2, the classical PDM model will be described. Theoretical analyses of VR in the PDM systems are presented in Section 3. Section 4 discusses our numerical simulations and Section 5 summarizes the results and draws conclusions.

2. Position-Dependent Mass Oscillators

We consider a classical oscillator whose dynamics may be described by the Lagrangian function [20]

$$L(x, \dot{x}; t) = T - V(x) = \frac{1}{2}m(x)\dot{x}^2 - V(x), \qquad (2.1)$$

where $T = \frac{1}{2}m(x)\dot{x}^2$ is the kinetic energy of the system, $V(x)$ is the system's potential, and $m(x)$ is an explicitly position-dependent mass function with x being its position at time t. In the analysis that follows, we assume a Duffing-type oscillator potential, i.e.

$$V_d(x) = \frac{1}{2}m(x)\omega_0^2 x^2 + \frac{1}{4}\beta x^4, \qquad (2.2)$$

where β is the potential parameter i.e. the system's coefficient of nonlinearity and ω_0 is the oscillator's natural frequency. The associated Euler-Lagrange equation can be written as

$$\frac{d}{dt}\left(\frac{\partial L}{\partial \dot{x}}\right) - \frac{\partial L}{\partial x} = \phi, \qquad (2.3)$$

where ϕ accounts for all the external contributions to the motion from dissipative and driving forces, assumed here to be $\phi = -\alpha\dot{x} + f\cos\omega t + g\cos\Omega t$. α is the damping coefficient and the amplitudes and frequencies of the external driving signals are f and ω for the weak component and g and Ω for the fast component, respectively. Using the Lagrangian function (2.1) in the Euler-Lagrange Eq. (2.3), the corresponding Newton's equation of motion may be written as

$$m(x)\ddot{x} + \frac{1}{2}m'(x)\dot{x}^2 + \frac{dV(x)}{dx} = \phi. \qquad (2.4)$$

The prime in Eq. (2.4) implies differentiation with respect to space variable x and the overdot indicates differentiation with respect to time.

As mentioned in the Introduction, Section 1, the nature of the problem or potential function considered determines the type of mass variation functions to be employed [14]. For instance, $m(x)$ can be a quadratic or exponential function of position x [20,102,103]. The former has been classified on the basis of its singularity property: as either regular mass-functions without singularity or as singular mass-functions with single or dual singularities [20]. Moreover, a classification of finite-gap PDM systems with diverse physical applications, such as the families of trigonometric, hyperbolic, and elliptic mass functions was presented in Ref. [15]. In this paper, we adopt the simplest regular mass-function without singularities:

$$m(x) = \frac{m_0}{1 + \lambda x^2}, \qquad (2.5)$$

originally proposed by Mathews and Lakshmanan [14] in relation to relativistic fields of elementary particles. The mass-function (2.5) appears frequently in the modelling of diverse nonlinear mechanical systems(See Refs. [19,20] and references therein). Here, m_0 is a constant mass, equivalent to the mass amplitude, and λ is the strength of the spatial nonlinearity in mass. $m(x)$ is bounded and defined over the entire real line $D(m_1) = \Re$ with its maximum, m_0, at $x = 0$ and varnishing as $|x| \to \infty$.

One can easily show that the equation of motion of the PDM-Duffing oscillator can be written as

$$m(x)\ddot{x} - m^2(x)\gamma\lambda x\dot{x}^2 + \alpha\dot{x} + m^2(x)\gamma\omega_0^2 x + \beta x^3 = f\cos\omega t + g\cos\Omega t, \qquad (2.6)$$

where $\gamma = \frac{1}{m_0}$. Remarkably, the PDM-Duffing oscillator (Eq. (2.6)) is consistent with the system described by Equation (23) in Ref. [19] for a unit mass amplitude ($m_0 = 1$) and $g = 0$. When the strength of nonlinearity in mass is negligible, that is $\lambda = 0$, Eq. (2.6) reduces to the well-studied bi-harmonically driven Duffing oscillator (equation (1) in Ref. [23]). Thus, the PDM system is a generalised version of the model systems considered hitherto in the study of VR. A typical example of a physical system described by Eq. (2.6) is a dual-frequency-driven gas bubble in which the mass of the bubble is dependent on the bubble's radius – which is a spatial coordinate [104]. The dual-frequency driving force, which can be realized by means of acoustic

waves with two frequency components, is applied to control the bubble's properties, including the promotion of acoustic cavitation. We refer the reader to a very recent study of driven bubbles highlighting the state-of-the art in applications of dual-frequency irradiation [105]. Moreover, the optical properties of semiconductor devices, such as $Al_xGa_{1-x}As/GaAs$, many of which are also characterised by position-dependent effective masses [8,9], can be modulated and controlled effectively by employing external fields consisting of an applied electromagnetic field and a high-frequency intense laser field (ILF). The quantum mechanical counterpart of VR [75,76] would of course be more appropriate for the analysis of the combined impacts of the position-dependent effective mass (PDEM) and applied fields on the properties of semiconductors.

In what follows, we will express Eq. (2.6) in a form that makes our analytical procedure convenient for the application of the well-established method of separation of motions (MSM). This is the basis of the theoretical analysis. For a nonlinear system whose mass depends explicitly on position or velocity, or both, intuitively one would encounter a position-dependent function $(k_1 \pm k_2 x^p)^n$, where k_1 and k_2 are constants, and p and n are positive and negative integers, respectively. This function cannot fit into the general framework of MSM. By dividing Eq. (2.6) by $m(x)$ we express it as,

$$
\begin{aligned}
\ddot{x} \quad - \quad & m_0(1+\lambda x^2)^{-1}(\gamma\lambda x\dot{x}^2 - \gamma\omega_0^2 x) + \gamma(1+\lambda x^2)(\alpha\dot{x} + \beta x^3) \\
& = \gamma(1+\lambda x^2)(f\cos\omega t + g\cos\Omega t).
\end{aligned}
\tag{2.7}
$$

and obtain $(k_1 \pm k_2 x^p)^n = (1+\lambda x)^{-1}$ which can be approximated using the Binomial expansion. Considering only the first three terms of the binomial expansion of $(1+\lambda x^2)^{-1}$, we write Eq. (2.7) as

$$
\begin{aligned}
\ddot{x} - m_0(1 - \lambda x^2 + \lambda^2 x^4)(\gamma\lambda x\dot{x}^2 \quad - \quad & \gamma\omega_0^2 x) + \gamma(1+\lambda x^2)(\alpha\dot{x} + \beta x^3) \\
& = \gamma(1+\lambda x^2)(f\cos\omega t + g\cos\Omega t).
\end{aligned}
\tag{2.8}
$$

Furthermore, by setting $\delta = \beta\gamma - \lambda\omega_0^2$, and $\xi = \beta\gamma\lambda + \lambda^2\omega_0^2$, in Eq. (2.8), the PDM-Duffing oscillator can be expressed in the form

$$
\begin{aligned}
\ddot{x} - \lambda(x - \lambda x^3 + \lambda^2 x^5)\dot{x}^2 \quad + \quad & \alpha\gamma(1+\lambda x^2)\dot{x} + \omega_0^2 x + \delta x^3 + \xi x^5 \\
= \quad & \gamma(1+\lambda x^2)(f\cos\omega t + g\cos\Omega t).
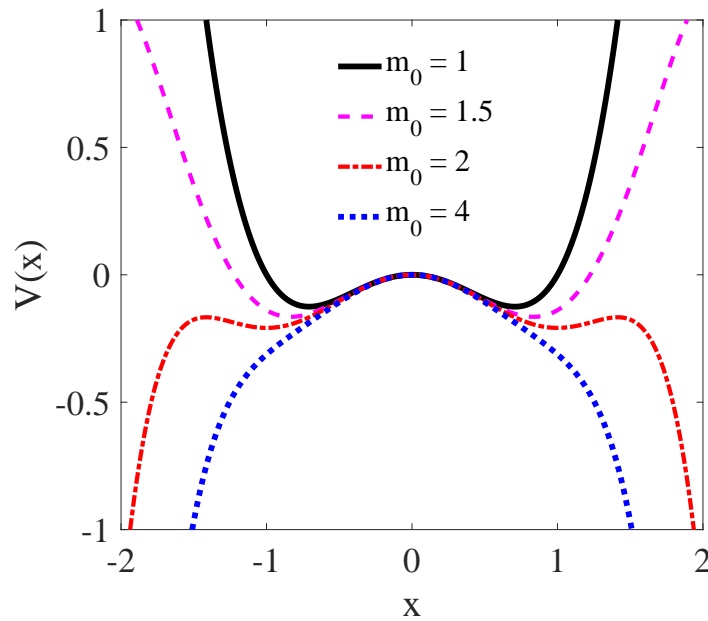\end{aligned}
\tag{2.9}
$$

The corresponding potential $V(x)$ of the system is

$$
V(x) = \frac{\omega_0^2}{2}x^2 + \frac{\delta}{4}x^4 + \frac{\xi}{6}x^6.
\tag{2.10}
$$

Henceforth, we shall refer to Eq. (2.9) as the PDM-Duffing oscillator. The system potential shown in Figs. 1 and 2 for different values of the PDM parameters: the mass amplitude $m_0(= 1, 1.5, 2, 4)$ and the strength of spatial nonlinearity $\lambda(= 0, 1, 1.5, 2)$, respectively, is computed from Eq. (2.10). The dynamical properties of the system can be altered by adjustment of its potential which, in turn, is largely determined by the PDM parameters (m_0, λ). We choose mass parameter regimes within which the system potential is double-well, so that $0 < m_0 < 1.5$ and $0 < \lambda < 1$ for $\alpha = 0.2$, $\beta = 1$, $\omega_0^2 = -1$.

3. Theoretical analysis

We now apply the standard MSM perturbation method, where the system's dynamics is assumed to be comprised of a slow component $y(t)$ and a fast component $z(t, \tau)$. The MSM method is used to derive two integro-differential equations in each component such that the superposition of their solutions completely solves the main equation of the system (Eq. (2.9)). Thus, defining

Figure 1. The system potential (Eq. (2.10)) for $\alpha = 0.2$, $\beta = 1$, $\omega_0^2 = -1$, $\lambda = 1$, $m_0 = 1, 1.5, 2, 4$,

$x = y + z$, and after factorizing like terms, the PDM-Duffing Eq. (2.9) can be re-written as

$$
\begin{aligned}
\ddot{y} \quad + \quad & \ddot{z} - \lambda(\lambda^2 y^5 + (5\lambda^2 z)y^4 + (10\lambda^2 z^2 - \lambda)y^3 + (10\lambda^2 z^3 - 3\lambda z)y^2 + (5\lambda^2 z^4 - 3\lambda z^2 + 1)y \\
+ \quad & \lambda^2 z^5 - \lambda z^3 + z)(\dot{y}^2 + 2\dot{y}\dot{z} + \dot{z}^2) + \alpha\gamma(1 + \lambda(y^2 + 2yz + z^2))(\dot{y} + \dot{z}) + \xi y^5 + 5\xi z y^4 \\
+ \quad & (10\xi z^2 + \delta)y^3 + (10\xi z^3 + 3\delta z)y^2 + (\omega_0^2 + 5\xi z^4 + 3\delta z^2)y + \omega_0^2 z + \delta z^3 + \xi z^5 \\
= \quad & \gamma(1 + \lambda(y^2 + 2yz + z^2))(f\cos\omega t + g\cos\Omega t).
\end{aligned}
\tag{3.1}
$$

By further expansion of Eq. 3.1, and considering that the fast signal z is rapidly oscillating with period $\frac{2\pi}{\Omega}$, we have

$$
\begin{aligned}
\ddot{y} \quad - \quad & \lambda(\lambda^2 y^5 + 5\lambda^2 \overline{z} y^4 + (10\lambda^2 \overline{z^2} - \lambda)y^3 + (10\lambda^2 \overline{z^3} - 3\lambda\overline{z})y^2 + (5\lambda^2 \overline{z^4} - 3\lambda\overline{z^2} + 1)y \\
+ \quad & \lambda^2 \overline{z^5} - \lambda\overline{z^3} + \overline{z})(\dot{y}^2 + \overline{\dot{z}^2}) + \alpha\gamma(1 + \lambda(y^2 + 2y\overline{z} + \overline{z^2}))\dot{y} + \xi y^5 + 5\xi\overline{z} y^4 \\
+ \quad & (10\xi\overline{z^2} + \delta)y^3 + (10\xi\overline{z^3} + 3\delta\overline{z})y^2 + (\omega_0^2 + 5\xi\overline{z^4} + 3\delta\overline{z^2})y + \omega_0^2\overline{z} + \delta\overline{z^3} + \xi\overline{z^5} \\
= \quad & \gamma(1 + \lambda(y^2 + 2y\overline{z} + \overline{z^2}))(f\cos\omega t + \overline{g\cos\Omega t}).
\end{aligned}
\tag{3.2}
$$

The mean value of z w.r.t fast time τ is given by

$$
\bar{z} = \frac{1}{2\pi}\int_0^{2\pi} z\,d\tau = 0,
\tag{3.3}
$$

so that Eq. (3.2) becomes

$$
\begin{aligned}
\ddot{y} \quad - \quad & \lambda(\lambda^2 y^5 + (10\lambda^2 \overline{z^2} - \lambda)y^3 + 10\lambda^2\overline{z^3} y^2 + (5\lambda^2 \overline{z^4} - 3\lambda\overline{z^2} + 1)y + \lambda^2 \overline{z^5} - \lambda\overline{z^3})(\dot{y}^2 + \overline{\dot{z}^2}) \\
+ \quad & \alpha\gamma(1 + \lambda(y^2 + \overline{z^2}))\dot{y} + \xi y^5 + (10\xi\overline{z^2} + \delta)y^3 + 10\xi\overline{z^3} y^2 + (\omega_0^2 + 5\xi\overline{z^4} + 3\delta\overline{z^2})y + \delta\overline{z^3} + \xi\overline{z^5} \\
= \quad & \gamma(1 + \lambda(y^2 + \overline{z^2}))f\cos\omega t.
\end{aligned}
\tag{3.4}
$$

Eq.(3.4) is the system's equation of slow motion, in which we are primarily interested.

An approximation method is used to determine the averages in the equation of slow motion. This is done by first obtaining the equation of fast oscillation in z by subtracting the equation

of the slow component y (Eq.(3.4)) from equation (3.1) for the composite system x. Hence, the system's equation of fast oscillation gives

$$
\begin{aligned}
\ddot{z} \;-\; & (2\dot{y}\lambda(\lambda^2 y^5 + (5\lambda^2 z)y^4 + (10\lambda^2 z^2 - \lambda)y^3 + (10\lambda^2 z^3 - 3\lambda z)y^2 + (5\lambda^2 z^4 - 3\lambda z^2 + 1)y \\
+\; & \lambda^2 z^5 - \lambda z^3 + z) + \alpha\gamma(1 + \lambda(y+z)^2))\dot{z} + \lambda^2(\dot{z}^2 - \overline{\dot{z}^2})y^5 + 5\lambda^2(z\dot{z}^2 - \overline{z}\,\overline{\dot{z}^2})y^4 \\
+\; & (10\lambda^2(z^2\dot{z}^2 - z^2\overline{\dot{z}^2}) - \lambda(\dot{z}^2 - \overline{\dot{z}^2}))y^3 + (10\lambda^2(z^3\dot{z}^2 - z^3\overline{\dot{z}^2}) - 3\lambda(z\dot{z}^2 - \overline{z}\,\overline{\dot{z}^2}))y^2 \\
+\; & (5\lambda^2(z^4\dot{z}^2 - z^4\overline{\dot{z}^2}) - 3\lambda(z^2\dot{z}^2 - z^2\overline{\dot{z}^2}) + (\dot{z}^2 - \overline{\dot{z}^2}))y + \lambda^2(z^5\dot{z}^2 - z^5\overline{\dot{z}^2}) - \lambda(z^3\dot{z}^2 - z^3\overline{\dot{z}^2}) \\
+\; & (z\dot{z}^2 - \overline{z}\,\overline{\dot{z}^2}) + (\dot{y}^2(5\lambda^2 y^4 - 3\lambda y^2 + 1) + 2\alpha\gamma\lambda y\dot{y} + 5\xi y^4 + 3\delta y^2 + \omega_0^2)(z - \overline{z}) \\
+\; & (\dot{y}^2(10\lambda^2 y^3 - 3\lambda) + 2\alpha\gamma\lambda y\dot{y} + 10\xi y^3 + 3\delta y)(z^2 - \overline{z^2}) \\
+\; & (\dot{y}^2(10\lambda^2 y^2 - \lambda) + 10\xi y^2 + \delta)(z^3 - \overline{z^3}) + (\dot{y}^2 5\lambda^2 + 5\xi y)(z^4 - \overline{z^4}) + (\dot{y}^2\lambda^2 + \xi)(z^5 - \overline{z^5}) \\
=\; & \gamma(1 + \lambda(y+z)^2)(g\cos\Omega t) + \gamma\lambda(2y(z - \overline{z}) + (z^2 - \overline{z^2}))(f\cos\omega t)
\end{aligned} \tag{3.5}
$$
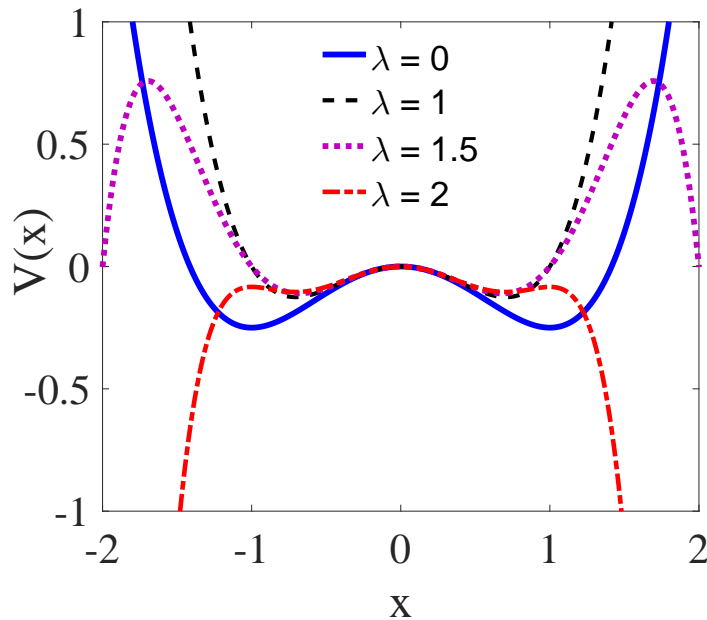
Figure 2. The system potential (Eq. (2.10)) for $m_0 = 1$, $\alpha = 0.2$, $\beta = 1$, $\omega_0^2 = -1$ and $\lambda = [0, 1, 1.5, 2]$.

We note that Eqns. (3.4) and (3.5) are a pair of integro-differential equations which describe the equations of slow oscillations y and fast vibrations z, respectively, and their superposition completely solves the composite system (Eq. (2.9)). Next, we apply the inertial approximation $\ddot{z} \gg \dot{z} \gg z \gg z^2$, by assuming the component z is much faster than the slow component y, so that y and $\dot{y}$ are considered as constants in Eq. (3.5). Hence Eq. (3.5) is reduced to
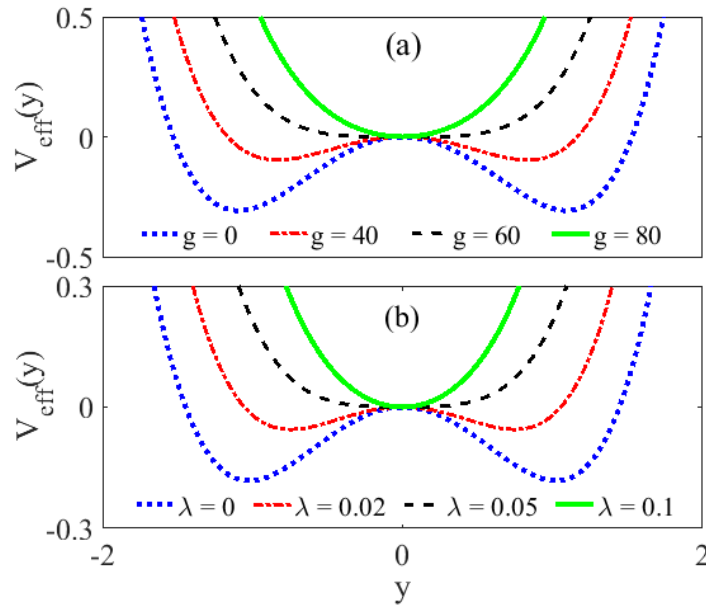
$$
\ddot{z} = \gamma g \cos\Omega t, \tag{3.6}
$$

which has a solution

$$
z = -\frac{\gamma g}{\Omega^2}\cos\Omega t, \tag{3.7}
$$

leading to the mean values

$$
\overline{z} = \overline{z^3} = \overline{z^5} = 0, \quad \overline{z^2} = \frac{\gamma^2 g^2}{2\Omega^4}, \quad \overline{z^4} = \frac{3\gamma^4 g^4}{8\Omega^8}, \quad \overline{\dot{z}^2} = \frac{\gamma^2 g^2}{2\Omega^2}. \tag{3.8}
$$

Figure 3. The effective potential (Eqn. (3.13)) for (a) $\lambda = 0.1$ and different values of $g(= 0, 40, 60, 80)$; (b) $g = 80$ and different values of $\lambda(= 0, 0.02, 0.05, 0.1)$. Other parameters are set as: $m_0 = 1.5$, $\Omega = 9.842$, $\alpha = 0.2$, $\beta = 1$, $\omega_0^2 = -1$

Using Eq. (3.8) in Eq. (3.4), the equation of motion for the slow component becomes

$$
\begin{aligned}
\ddot{y} \quad &- \quad \lambda(\lambda^2 y^5 + (10\lambda^2 \overline{z^2} - \lambda)y^3 + (5\lambda^2 \overline{z^4} - 3\lambda\overline{z^2} + 1)y)(\dot{y}^2 + \overline{\dot{z}^2}) + \alpha\gamma(1 + \lambda(y^2 + \overline{z^2}))\dot{y} \\
&+ \quad \xi y^5 + (10\xi\overline{z^2} + \delta)y^3 + (\omega_0^2 + 5\xi\overline{z^4} + 3\delta\overline{z^2})y = \gamma(1 + \lambda(y^2 + \overline{z^2}))f\cos\omega t. \quad (3.9)
\end{aligned}
$$

Eq. (3.9) can be simplified by collecting terms in y as

$$
\begin{aligned}
\ddot{y} \quad &- \quad \lambda(\lambda^2 y^5 + (10\lambda^2 \overline{z^2} - \lambda)y^3 + (5\lambda^2 \overline{z^4} - 3\lambda\overline{z^2} + 1)y)(\dot{y}^2) + \alpha\gamma(1 + \lambda(y^2 + \overline{z^2}))\dot{y} \\
&+ \quad (\lambda(5\lambda^2 \overline{z^4} - 3\lambda\overline{z^2} + 1)\overline{\dot{z}^2} + \omega_0^2 + 5\xi\overline{z^4} + 3\delta\overline{z^2})y \\
&+ \quad (\lambda(10\lambda^2 \overline{z^2} - \lambda)\overline{\dot{z}^2} + (10\xi\overline{z^2} + \delta))y^3 + (\lambda^3 \overline{\dot{z}^2} + \xi)y^5 = \gamma(1 + \lambda(y^2 + \overline{z^2}))f\cos\omega t \quad (3.10)
\end{aligned}
$$

By setting

$$
\begin{aligned}
C_1 \quad &= \quad 5\lambda^2 \overline{z^4} - 3\lambda\overline{z^2} + 1 = \frac{15\lambda^2 \gamma^4 g^4}{8\Omega^8} - \frac{3\lambda\gamma^2 g^2}{2\Omega^4} + 1, \; C_2 = 10\lambda^2 \overline{z^2} - \lambda = \frac{5\lambda^2 \gamma^2 g^2}{\Omega^4} - \lambda, \\
C_3 \quad &= \quad 1 + \lambda\overline{z^2} = 1 + \frac{\lambda\gamma^2 g^2}{2\Omega^4}, \\
\eta_1 \quad &= \quad \lambda C_1 \overline{\dot{z}^2} + \omega_0^2 + 5\xi\overline{z^4} + 3\delta\overline{z^2} = \frac{\lambda C_1 \gamma^2 g^2}{2\Omega^2} + \omega_0^2 + \frac{15\xi\gamma^4 g^4}{8\Omega^8} + \frac{3\delta\gamma^2 g^2}{2\Omega^4}, \\
\eta_2 \quad &= \quad \lambda C_2 \overline{\dot{z}^2} + 10\xi\overline{z^2} + \delta = \frac{\lambda C_2 \gamma^2 g^2}{2\Omega^2} + \frac{5\xi\gamma^2 g^2}{\Omega^4} + \delta, \; \eta_3 = \lambda^3 \overline{\dot{z}^2} + \xi = \frac{\lambda^3 \gamma^2 g^2}{2\Omega^2} + \xi, \quad (3.11)
\end{aligned}
$$

the system's slow oscillation described by Eqn(3.4) can be written as

$$
\ddot{y} - \lambda(C_1 y + C_2 y^3 + \lambda^2 y^5)\dot{y}^2 + \alpha\gamma(C_3 + \lambda y^2)\dot{y} + \eta_1 y + \eta_2 y^3 + \eta_3 y^5 = \gamma(C_3 + \lambda y^2)f\cos\omega t \quad (3.12)
$$

Thus, the effective potential of the system is given by

$$
V_{eff}(y) = \frac{\eta_1}{2}y^2 + \frac{\eta_2}{4}y^4 + \frac{\eta_3}{6}y^6. \quad (3.13)
$$

The slow oscillation takes place about one of the equilibrium points

$$y_1^* = 0, \ y_{2,3}^* = \pm\sqrt{\frac{-\eta_2 + \sqrt{\eta_2^2 - 4\eta_1\eta_3}}{2\eta_3}}, \ y_{4,5}^* = \pm\sqrt{\frac{-\eta_2 - \sqrt{\eta_2^2 - 4\eta_1\eta_3}}{2\eta_3}}. \tag{3.14}$$

The choice of the system parameters $\omega^2, \beta, m_0, \lambda, g$ and Ω determines the shape and depth of the effective potential since the magnitude and the signs of η_1, η_2 and η_3 can be changed by varying them. Thus, the structure of $V_{eff}(y)$ can change depending on the sign of η_1, η_2 and η_3 by varying any of the potential parameter (ω^2, β), HF parameters (g, Ω) or PDM parameters (m_0, λ). Different potential structures can be realized for different parameter choices. For instance, by assuming that $\eta_3 > 0$, the following cases arise:

Case I $\eta_1, \eta_2 > 0$, or $\eta_1 > 0, \eta_2 < 0$ with $\eta_2^2 < 4\eta_1\eta_3$. The only equilibrium point is y_1^*.
Case II $\eta_1 < 0, \eta_2$ - arbitrary. Three equilibrium points exist: $-y_1^*, y_{2,3}^*$.
Case III $\eta_1 > 0, \eta_2 < 0$ with $\eta_2^2 > 4\eta_1\eta_3$. Five equilibrium points exist: $-y_1^*, y_{2,3}^*, y_{4,5}^*$.

Clearly, the effective potential is not just dependent on the parameters of the fast driving signal, as is typical of the VR phenomenon, but also depends on the parameters $(m_0, \ \lambda)$ of the PDM – implying that either or both of the PDM parameters must make a significant contribution to the shapes of the resonances. The effective potential of the driven PDM-Duffing oscillator given by Eq. (3.13) is shown in Fig. 3(a) for four different values of the HF amplitude $g(= 0, 25, 40, 80)$ for the parameter values $m_0 = 1, \lambda = 0.1, \alpha = 0.2, \beta = 1, \omega_0^2 = -1$, and in Fig. 3(b) for four different values of the strength of spatial nonlinearity in mass $\lambda(= 0, 0.02, 0.05, 0.1)$ for the parameter values $g = 80, m_0 = 1.5, \alpha = 0.2, \beta = 1$ and $\omega_0^2 = -1$. By varying the HF amplitude, the shape and depth of $V_{eff}(y)$ can be altered from double-well (at $g = 0, \ 25, \ 40$) to single-well (at $g = 80$) by choice of the HF amplitude g, even when the PDM parameters (m_0, λ) are restricted to the regime $(m_0, \lambda) \in ((0, \ 1.5), (0, \ 1))$ where the system has a double-well potential in the absence of the HF signal. Additionally, in the presence of an HF signal, the shape and depth of the effective potential $V_{eff}(y)$ can be altered from single-well (when $\lambda = 0.05, 0.1$) to double-well (when $\lambda = 0, 0.02$) depending on the choice of strength of mass nonlinearity λ.

Next, we linearize Eq. (3.12) around the equilibrium points $(y^*, \dot{y}^*)$ in order to obtain an approximate analytic response amplitude Q_{ana} which can also be compared to the response amplitude Q_{num} obtained from the Fourier coefficients of the solution of the full equation of the system (2.9). The system's oscillation can be described in terms of the deviation of slow motion y from the equilibrium points y^* by using the deviation variable $Y = y - y^*$ in Eq. (3.12). This yields the motion around equilibrium points in the form

$$\begin{aligned}
\ddot{Y} \ &- \ \lambda(\Delta + \Delta_1 Y + \Delta_2 Y^2 + \Delta_3 Y^3 + \Delta_4 Y^4 + \lambda^2 Y^5)\dot{Y}^2 + \alpha\gamma(\Xi_1 + \Xi_2 Y + \lambda Y^2)\dot{Y} \\
&+ \ \Theta + \Theta_1 Y + \Theta_2 Y^2 + \Theta_3 Y^3 + \Theta_4 Y^4 + \eta_3 Y^5 = \gamma(\Xi_1 + \Xi_2 Y + \lambda Y^2)f\cos\omega t, \quad (3.15)
\end{aligned}$$

where

$$\begin{aligned}
\Delta \ &= \ C_1 y^* + C_2 y^{*3} + \lambda^2 y^{*5}, \Delta_1 = C_1 + 3C_2 y^{*2} + 5\lambda^2 y^{*4}, \Delta_2 = 3C_2 y^* + 10\lambda^2 y^{*2}, \\
\Delta_3 \ &= \ C_2 + 10\lambda^2 y^{*2}, \Delta_4 = 5\lambda^2 y^*, \Xi_1 = C_3 + \lambda y^{*2}, \Xi_2 = 2\lambda y^*, \\
\Theta \ &= \ \eta_1 y^* + \eta_2 y^{*3} + \eta_3 y^{*5}, \Theta_1 = \eta_1 + 3\eta_2 y^{*2} + 5\eta_3 y^{*4}, \\
\Theta_2 \ &= \ 3\eta_2 y^* + 10\eta_3 y^{*2}, \Theta_3 = \eta_2 + 10\eta_3 y^{*2}, \Theta_4 = 5\eta_3 y^*.
\end{aligned} \tag{3.16}$$

By ignoring the nonlinear parts of Eq. (3.15) and using the approximation $f \ll 1$ such that $|Y| \ll 1$ in the long-term limit $t \to \infty$, the linearized equation of motion then becomes

$$\ddot{Y} + \mu\dot{Y} + \omega_r^2 Y = F\cos\omega t, \tag{3.17}$$

where the resonant frequency is $\omega_r = \sqrt{\eta_1}$, $\mu = \alpha\gamma C_3$ and $F = \gamma C_3 f$ when the oscillation is considered around the equilibrium point $y^* = 0$. For $y^* \neq 0$, $\omega_r^2 = \Theta_1$, $\mu = \alpha\gamma\Xi_1$ and $F = \gamma(\Xi_1 + \Xi_2 Y + \lambda Y^2)f$. It is clear that the steady state solution of equation (3.12) takes the form

$$Y(t) = A_L \cos(\omega t + \Phi), \tag{3.18}$$

and that the response amplitude can be computed as

$$Q_{ana} = \frac{A_L}{f} = \frac{\gamma C_3}{\sqrt{(\omega_r^2 - \omega^2)^2 + \mu^2\omega^2}}, \tag{3.19}$$

If we set $S = (\omega_r^2 - \omega^2)^2 + \mu^2\omega^2$ in Eqn. (3.19), the qualitative features of Q_{ana} would be determined by S. A local minimum in S implies resonance, i.e. the appearance of a maximum in Q_{ana}. When a variation of any of the system parameters leads the system to resonance, the value of the parameter at which resonance occur (e.g. $\lambda = \lambda_{vr}$) can be obtained from the root of the equation $S_\lambda = \frac{dS}{d\lambda} = 0$ and $S_{\lambda\lambda}|_{\lambda=\lambda_{vr}} > 0$.

When the sign of either η_1 or η_2 is changed by varying any of g, Ω, m_0 or λ, the effective potential changes structure from single-well to double-well as shown in Fig. 3. The value of g_{vr} and λ_{vr} when the effective potential is a single-well can be obtained by setting $S_g = 0$ and $S_\lambda = 0$ and satisfies the condition:

$$g_{vr} = \begin{cases} \{\sqrt{z} \mid z \,\epsilon\, \sigma_1\} \cup \{-\sqrt{z} \mid z \,\epsilon\, \sigma_1\}, & \text{if } e \neq 0, \\[2mm] \pm\Omega^2\sqrt{\frac{-b \pm (\sigma_2 - d\Omega^2)}{\sigma_3}}, & \text{if } a \neq c\Omega^2 \wedge e = 0 \end{cases} \tag{3.20}$$

where

$$a = \frac{15\gamma^4\xi}{8}, \quad b = \frac{3\delta\gamma^2}{2}, \quad c = \frac{3\lambda 2\gamma^4}{4}, \quad d = \frac{15\gamma^4\xi}{8}, \quad e = 15\frac{\lambda^3\gamma^6}{16}, \quad f = \omega^2 - \omega_0^2,$$

$$\sigma_1 = \sqrt{(e z^3 - c\,\Omega^4 z^2 + a\,\Omega^2 z^2 + d\,\Omega^8 z + f\,\Omega^{10})},$$

$$\sigma_2 = \sqrt{b^2 + 2bd\Omega^2 + d^2\Omega^4 + 4cf\Omega^2 - 4af}, \quad \sigma_3 = 2(a - c\Omega^2). \tag{3.21}$$

In addition, the resonance condition for λ_{vr} gives

$$\lambda_{vr} = \begin{cases} \sqrt{(az^3 + b\Omega^4 z^2 - c\Omega^8 z + d\Omega^{10}, z)}, & \text{if } a \neq 0 \\[2mm] \frac{\Omega^3(c\Omega \pm \sqrt{c^2\Omega^2 - 4bd})}{2b}, & \text{if } a = 0 \wedge b \neq 0. \end{cases} \tag{3.22}$$

$$a = \frac{15\gamma^6 g^6}{16}, \quad b = \frac{3\gamma^4 g^4}{4}, \quad c = \frac{\gamma^2 g^2}{2}, \quad d = \frac{15\gamma^4\xi g^4}{8\Omega^8} + \frac{3\delta\gamma^2 g2}{2\Omega^4} + \omega^2 - \omega_0^2, \tag{3.23}$$

and

$$\omega_{vr} = \sqrt{\omega_r^2 - \frac{\mu}{2}}, \quad \omega_r^2 - \frac{\mu}{2}. \tag{3.24}$$

When the effective potential is a double-well, it is challenging to establish analytical conditions in terms of g_{vr} and λ_{vr}. However, they can be computed numerically by analysing the cases $\omega_r^2 - \omega^2 = 0$ and $\omega_{rg} = 0$ or $\omega_{r\lambda} = 0$ since $S_g = 0$ (or $S_\lambda = 0$) at resonance.

4. Numerical Results and Discussions

To validate the analytic results, the theoretical response amplitude Q given by Eq. (3.19) was compared with the numerical Q computed from the Fourier spectrum of the solution of the main PDM-Duffing equation (Eq. (2.9)) expressed as coupled first-order autonomous ordinary differential equations (ODEs) of the form:
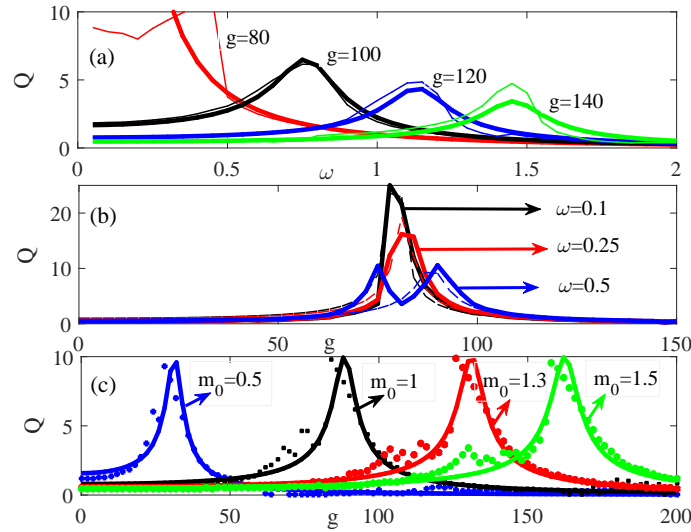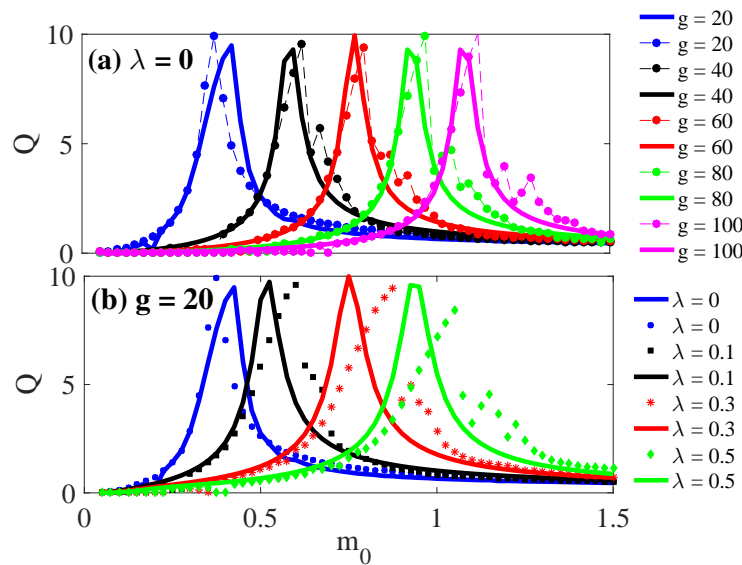
Figure 4. The variation of response amplitude Q with (a) ω for four values of HF amplitude g (80, 100, 120, 140) for a system with unit mass ($m_0 = 1, \lambda = 0$) and $f = 0.05$, (b) with HF amplitude g for three values of LF ω ($\omega = 0.1$, $\omega = 0.25$ and $\omega = 0.5$) for a system with unit mass ($m_0 = 1, \lambda = 0$) and $f = 0.01$, and (c) with g for five values of mass amplitudes $m_0 = (1, \ 1.1, \ 1.2, \ 1.3, \ 1.5)$ and $f = 0.05$ for a system with constant mass ($\lambda = 0$). Other parameters are set as: $\Omega = 9.842$, $\omega = 0.5$, $\alpha = 0.2$, $\beta = 1$, $\omega_0^2 = -1$. The thick lines represent analytically computed response amplitudes from Eq. (3.19) while thin lines, broken lines and markers of the same colour represent corresponding the numerically computed response amplitude from the main equation of the PDM-Duffing oscillator (Eq. (2.9)) using Eq. (4.5).

$$
\begin{aligned}
\frac{dx}{dt} &= y, \\
\frac{dy}{dt} &= \lambda(x - \lambda x^3 + \lambda^2 x^5)\dot{x}^2 - \alpha\gamma(1 + \lambda x^2)\dot{x} - \omega_0^2 x - \delta x^3 - \xi x^5 \\
&\quad + \gamma(1 + \lambda x^2)(f \cos \omega t + g \cos \Omega t).
\end{aligned}
\tag{4.1}
$$

The solution of Eq. (4.1), corresponding to the output signal of the system, is obtained by numerical integration using the fourth order Runge-Kutta (FORK) scheme with step size $\Delta t = 0.01T$ over a simulation time interval $T_s = nT$, where $T = \frac{2\pi}{\omega}$ is the period of the oscillation, ω is the low-frequency (LF) of the input signal and $n(= 1, 2, 3, \dots)$ is the number of complete oscillations. We used $(x(0), \dot{x}(0.1))$ initial conditions with a relaxation time of $20T$. Except where otherwise specified, the values of fixed system parameters were: $\alpha = 0.2$, $\beta = 1$, $\omega_0^2 = -1$, $\Omega = 9.842$, $\omega = 0.5$ and $f = 0.05$. The PDM parameters were set as $(m_0, \lambda) \in ((0, 1.5), (0, 1))$. These parameter choices ensure that the system remains in the overdamped regime for which only periodic or quasiperiodic motion is admissible and where the system remain a bistable oscillator. The other system parameters were chosen within regimes that optimize the emergence of VR for $n = 200$.

The response amplitude Q at frequency ω was then obtained from the Fourier sine and cosine coefficients of the output signal with components Q_s and Q_c given by

$$
Q_s = \frac{2}{nT} \int_0^{nT} x(t) \sin \omega t \, dt, \quad Q_c = \frac{2}{nT} \int_0^{nT} x(t) \cos \omega t \, dt.
\tag{4.2}
$$

Figure 5. The variation of response amplitude Q with (a) mass amplitude m_0 for four values HF amplitude g (= 20, 40, 60, 80, g = 100) for a system with mass independent of position ($\lambda = 0$). (b) mass amplitude m_0 for four values of strength of mass nonlinearity $\lambda (= 0, 0.1, 0.3, 0.5)$. Other parameters are set as: $\Omega = 9.842$, $\omega = 0.5$, $\alpha = 0.2$, $\beta = 1$, $\omega_0^2 = -1$, f = 0.05. The thick lines represent analytically computed response amplitudes from Eq. (3.19) while the thin lines, broken lines and markers represent the numerically computed response amplitude from the main equation of the PDM-Duffing oscillator (Eq. (2.9)) using Eq. (4.5).

Conventionally, the amplitude of the output signal is given by,

$$A = \sqrt{Q_s^2 + Q_c^2}. \tag{4.3}$$

while the phase shift is,

$$\Phi = \tan^{-1}\left(\frac{Q_s}{Q_c}\right). \tag{4.4}$$

The response amplitude is thus given by

$$Q_{num} = \frac{\sqrt{Q_s^2 + Q_c^2}}{f}. \tag{4.5}$$

The analytically computed response amplitudes from Eq. (3.19) (indicated by solid lines) are compared with the corresponding numerical response amplitudes (indicated by thin lines, broken lines or/and markers) computed directly from the main equation of the system (Eq. (2.9)) using Eq. (4.5) by superposing response curves for a range of system parameter.

   We begin by considering VR for a Duffing oscillator with a constant unitary unit mass, a special case for which $M(x) = 1$ [23,24,106]. Then, we extend it to the PDM-Duffing oscillator in which $m(x) = m_0$ and $\lambda = 0$, corresponding to a Duffing oscillator with constant mass. Remarkably, for a particle with constant unitary mass ($m_0 = 1$, $\lambda = 0$), the PDM-Duffing oscillator (Eq. (2.9) is reduced to the bistable oscillator considered in the pioneering work on VR by Landa and McClintock (2000) [23]. As expected for this special case, VR is observed as shown in Fig. 4. In fact, the results of the preliminary analysis for a PDM-Duffing system with constant unitary mass as presented in Fig. 4(a) are consistent with both the theoretical and numerical results presented by Blekhmann and Landa (2001) (see Fig. 2(b) of Ref. [106]). Further evidence of VR in this special
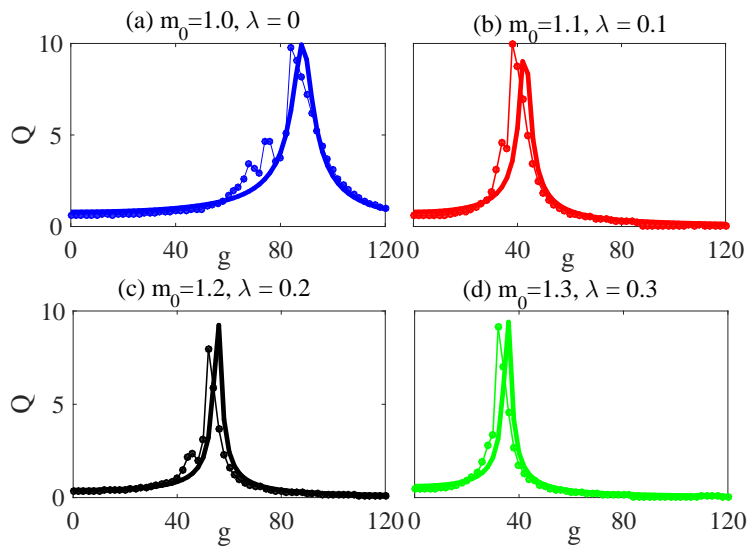
Figure 6. The dependence of response amplitude Q with g for system with position dependent mass for four different combinations of the mass amplitude m_0 and nonlinear strength λ, (a) $m_0 = 1, \lambda = 0$, (b) $m_0 = 1.1, \lambda = 0.1$, (c) $m_0 = 1.2, \lambda = 0.2$, (d) $m_0 = 1.3, \lambda = 0.3$. Other parameters are set as: $\Omega = 9.842, \omega = 0.5, \alpha = 0.2, \beta = 1, \omega_0^2 = -1$, f = 0.05. The thick lines represent analytically computed response amplitudes from Eq. (3.19) while the thin lines, broken lines and markers represent the numerically computed response amplitude from the main equation of the PDM-Duffing oscillator (Eq. (2.9)) using Eq. (4.5).
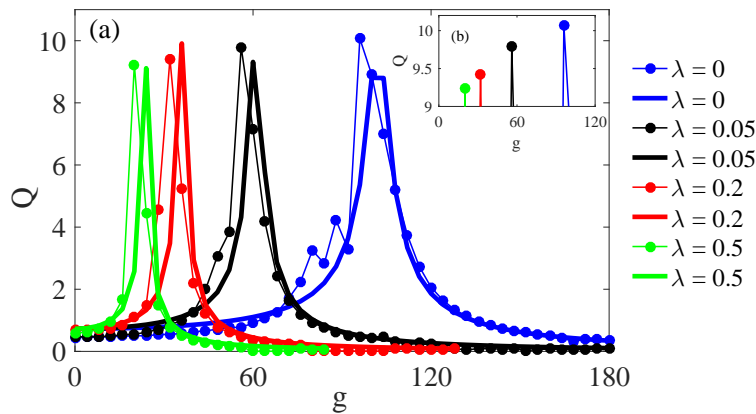
Figure 7. The dependence of response amplitude Q with g (a) for system with position dependent mass for four values mass nonlinear strength λ, ($\lambda = 0, \lambda = 0.05, \lambda = 0.2, \lambda = 0.5$) for mass amplitude $m_0 - 1.1$. (b)Inset shows reduction in maximum response amplitude Q_{max} with increasing values of the mass nonlinear strengths λ considered in (a). Other parameters are set as: $\Omega = 9.842, \omega = 0.5, \alpha = 0.2, \beta = 1, \omega_0^2 = -1, f = 0.05$. The thick lines represent analytically computed response amplitudes from Eq. (3.19) while the thin lines with markers represent the numerically computed response amplitude from the main equation of the PDM-Duffing oscillator (Eq. (2.9)) using Eq. (4.5).
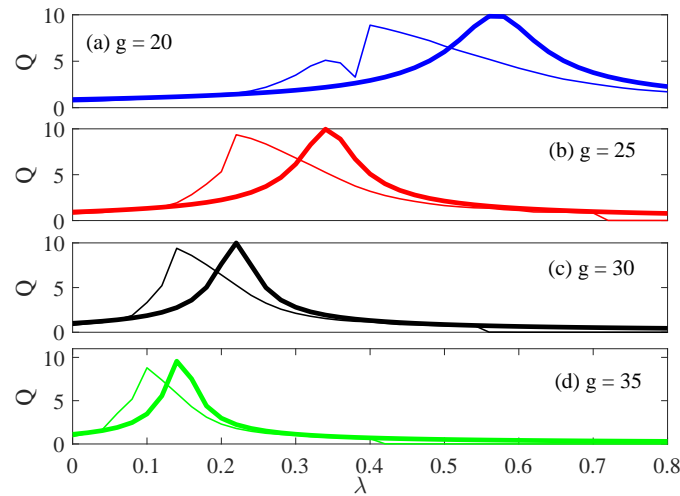
Figure 8. The dependence of response amplitude Q on strength of mass spatial nonlinearity λ for four values of HF force amplitude g presented in panels (a) $g = 20$, (b) $g = 25$, (c) $g = 30$, (d) $g = 35$, respectively for $m_0 = 1$. Other parameters are set as: $\Omega = 9.842$, $\omega = 0.5$, $\alpha = 0.2$, $\beta = 1$, $\omega_0^2 = -1$, $f = 0.05$. The thick lines represent analytically computed response amplitudes from Eq. (3.19) while the thin lines represent the numerically computed response amplitude from the main equation of the PDM-Duffing oscillator (Eq. (2.9)) using Eq. (4.5).

case is presented for the dependence of the response amplitude Q on the HF amplitude g for three values of the LF $\omega(= 0.1, 0.25, 0.1)$, as shown in Fig. 4(b) for $f = 0.01$.

Next we consider the effect of the PDM parameters on the observed resonances and thus focus on the possible impact of the mass parameters m_0 and λ. First we consider the effect of the mass amplitude m_0 on known resonances for the preliminary case $\lambda = 0$, as presented in Fig. 4(c) for the variation of the response amplitude Q with HF amplitude g for the constant unitary mass $m_0 = 1$ and three larger and smaller values ($m_0 = 0.5, m_0 = 1.3, m_0 = 1.5$) for $f = 0.05$ and other parameters unchanged. In Fig. 4(c), for $m_0 = 1$ and $\omega = 0.5$ the resonance curve confirms the response curve presented by Landa and McClintock [23] (see Curve 2 of Figure 2(a), left panel). The VR phenomenon also exists for the other mass amplitudes considered (in Fig. 4(c)), with no significant enhancement as m_0 increases but with a marked shift in the HF amplitude value for which Q is maximum. As m_0 increases, this optimal HF amplitude value $g(Q_{max})$ also increases. Thus, for a Duffing oscillator with a unitary particle mass, the mass amplitude plays a complementary role to the HF signal parameters (g, Ω) in the observed resonances.

Furthermore, the possibility of initiating resonance through variation of the PDM mass amplitude, with the cooperation of the HF input signal, is confirmed by the results presented in Fig. 5. Fig. 5(a) shows the dependence of the response amplitude Q on m_0 for four values of the HF amplitude $g(= 20, 40, 60, 80, 100)$ for a particle with constant mass ($\lambda = 0$). Resonances with single peaks at $m_0(Q_{max})$ directly dependent on the HF amplitude g can be seen for each value of g. Although resonances can thus be achieved by varying g, there is no significant optimization, and the impact of g on Q is a shift in the peak position in the direction of increasing m_0. In addition, by switching on the mass spatial nonlinearity and examining the dependence of Q on m_0 for increasing mass nonlinearity ($\lambda = 0$, $\lambda = 0.1$, $\lambda = 0.2$, $\lambda = 0.5$) at $g = 20$, single resonance peaks indicative of VR for the dependence of Q on g (or Ω, shown in Fig. 4(b)) are observed for each value of λ. It is evident that the mass amplitude m_0 can be used to initiate VR or/and can complement the HF input signal parameters in determining the conditions for resonance. This is similar to the effect of constant mass on the VR phenomenon observed in the dynamics of

an inhomogeneously damped one-dimensional single particle moving in a symmetrical periodic potential [37,101]. For the observed resonances in Fig. 5, the PDM mass amplitude m_0 and the HF signal amplitude g are directly related: increasing the value of g corresponds to increasing the value of mass amplitude m_0.

To gain further insight into the contributions of the position-dependent mass to VR, we also considered the effect of the PDM nonlinear strength λ on the observed resonances. First, we showed that the resonances for constant unitary mass can also be realized with a suitable combination of PDM parameters when the mass spatial nonlinearity is activated. This is presented in Fig. 6(a)-(d) for varying HF amplitude g and for four different combinations of the PDM parameters $(m_0, \lambda) \in (1, 0), (1.1, 0.1), (1.2, 0.2), (1.3, 0.3)$, respectively for $f = 0.05$. As shown in Fig. 6(b)-(d), VR is observed for combinations of the PDM parameters other than the simple case shown in Fig. 6(a). This implies that, besides the independent impact of the mass amplitude m_0, the combination of PDM parameters plays a role in determining the conditions for VR. The variation of the response amplitude Q with HF amplitude g for four values of spatial nonlinearity strength λ ($\lambda = 0$, $\lambda = 0.05$, $\lambda = 0.2$, $\lambda = 0.5$) is presented in Fig. 7 for $m_0 = 1.1$. The shape of the resonance curve, maximum response amplitude Q_{max}, and $g(Q_{max})$ all depend on λ. The maximum response amplitude Q_{max} at which VR occurs decreases with increase in the strength of the spatial nonlinearity, as presented in the inset (b) of Fig. 7. Here, we have zoomed the top portions of the numerically computed response curves, i.e. Fig. 7(a).

Finally, Fig. 8 demonstrates that cooperation between the HF input signal and the PDM parameters can induce VR through the mass spatial nonlinearity strength λ for $m_0 = 1$. This is presented for four values of the HF input signal amplitude $g(g = 20, g = 25, g = 30, g = 35)$ in panels (a) - (d) of Fig. 8, respectively. The observed single resonances are typical of VR induced by the HF input parameters. In this figure, resonance occurs for a pair of low values of λ and high values of g, illustrating the cooperation effect between the HF driving force and the PDM in the VR process. In general, the strength of the spatial nonlinearity optimizes the effect of HF amplitude when the system is driven into resonance and *vice-versa*.

In Fig. 9, we present a 3-dimensional plot illustrating the numerically computed response amplitude Q as functions of both the strength of the mass nonlinearity λ and the HF signal amplitude g for ω ($= 0.1, 0.25, 0.5, 1.0$), respectively. The occurrence of VR is demonstrated in Fig. 4(b) for a PDM oscillator with constant mass ($m_0 = 1$, $\lambda = 0$) by varying the HF amplitude g for three values of ω ($= 0.1, 0.25, 0.5$). Other parameters are set as stated for Fig. 4(b). Clearly, "hills" corresponding to high values of the response amplitude Q, stretching along λ and spreading into the (g, λ)-plane show the occurrence of single resonance at $\omega = 0.1$ and $\omega = 0.25$ (shown in Fig. 9(a) and (b), respectively). As ω assumes larger values, double-peaked "hills" appear simultaneously as shown in Fig. 9(d) for $\omega = 1$. The value of the mass nonlinear strength λ determines the occurrence of either single or double-peaked resonances with $\omega = 0.5$ as shown in Fig. 9(c). For $\lambda = 0$, Fig. 9(a)–(c) provides a clearer picture of the features depicted in Fig. 4(b) in relation to the occurrence of VR in the system and, in addition, demonstrates the possibility of obtaining VR at other values of mass nonlinear strength ($0 < \lambda \leq 0.8$). Thus, salient features of the superposed resonance curves in Fig. 4(b) are validated by Fig. 9(a)–(c) including: (i) the reduction in the value of Q_{max} when ω which can be seen by comparing the maximum response amplitudes in Fig. 9((a) to (c)); and (ii) the appearance of single-peaked resonance in Fig. 4(b) when $\omega = 0.1$ and $\omega = 0.25$ and double-peaked resonances at $\omega = 0.5$. In the 3D plot of Fig. 9, the above details are obvious with a single-peaked resonance appearing when $\lambda = 0$ in Fig. 9(a) and (b) and double-peaked resonances when $\lambda \simeq 0$ in Fig. 9(c). Further increase in the value of ω to $\omega = 1$ results in sustained double-peaked resonances for all values of mass nonlinear strength $0 \leq \lambda \leq 0.8$ as shown in Fig. 9(d). Note that in Fig. 3 the effective potential changes from a double-well structure (for $g = 0$) to a single-well structure as g takes on larger values, such that $g \geq 80$. The transition to double-well structure is readily enhanced by the cooperation between the PDM parameter λ and the high-frequency amplitude g.
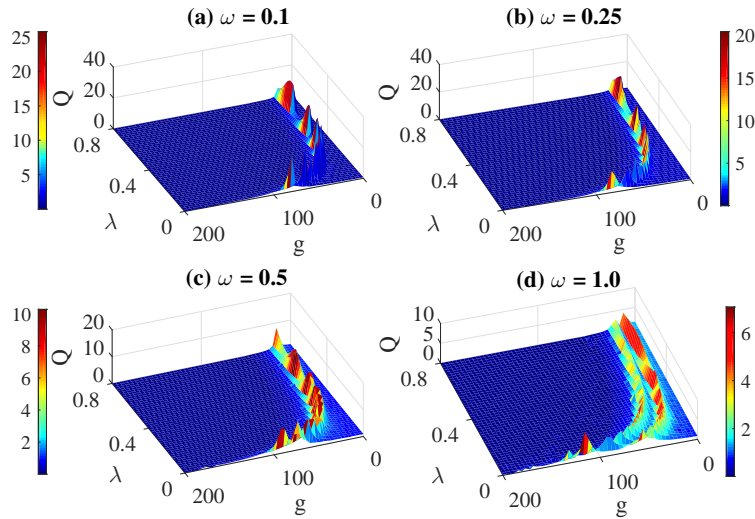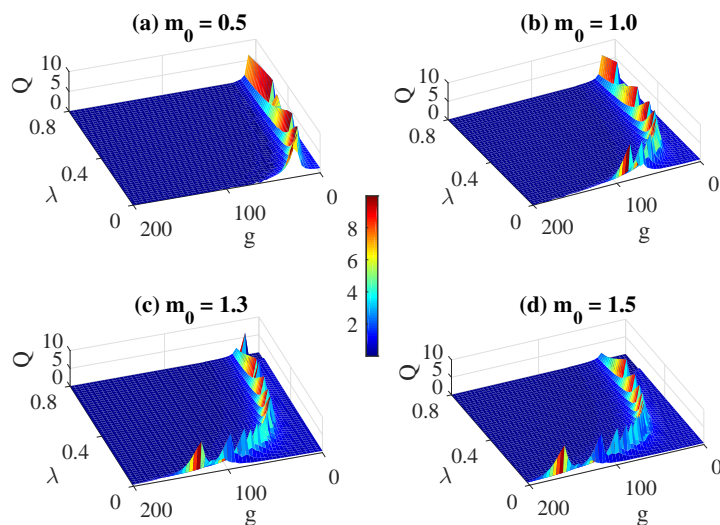
Figure 9. [Color Online] The dependence of the numerically computed response amplitude Q on the strength of mass nonlinearity λ and the HF signal amplitude g for four values of the low frequency ω: ($\omega = 0.1$, $\omega = 0.25$, $\omega = 0.5$, $\omega = 1.0$) shown in (a)–(d), respectively. Other parameters are set as: $\Omega = 9.842$, $m_0 = 1$, $\alpha = 0.2$, $\beta = 1$, $\omega_0^2 = -1$, $f = 0.01$.

Fig. 10 presents a broader picture of the effect of the PDM parameters (λ, m_0) on the system's response amplitude Q. Here, Q was also computed numerically. It is plotted in 3D as functions of both the strength of the mass nonlinearity λ and the amplitude g for four values of mass amplitude: $m_0 = 0.5$, $m_0 = 1$, $m_0 = 1.5$, $m_0 = 1.5$ in panels (a)–(d), respectively, for $f = 0.05$. Resonance peaks take the form of ridge-shaped "hills", stretching along λ parameter values and spreading across the (g, λ)-plane when m_0 is increased, as shown in Fig. 10(a)–(d). The results clearly indicate the continuous occurrence of single resonance peaks. Indeed a slice of Fig. 10 along $\lambda = 0$ is consistent with Fig. 4(c) in terms of the values of amplitude g at which resonances occur. There is also a correspondence between the increase in the value of the HF signal amplitude and the increase in the mass amplitude m_0, as indicated in Fig. 4(c) and Fig. 5. This correspondence can be generalized for all values of $\lambda \in (0, 0.8)$. Moreover, the occurrence of resonance for different combinations of PDM parameters as presented in fig. 6 for four combinations of PDM parameters is also illustrated in Fig. 10. The inverse relationship between the response amplitude Q and the strength of mass nonlinearity λ as depicted in Fig. 7 and Fig. 8 for $m_0 = 1$ can be validated by considering the values of g where resonances occur along the λ-axis in Fig. 10(b). This inverse relationship between g_{VR} and λ_{VR} becomes pronounced with increasing values of m_0 ($m_0 = 0.5$, 1.0, 1.3, 1.5) as shown in Fig. 10(a)-(d), and manifests as a gradual spread in the resonance hills from one end (as shown in Fig. 10(a) when $m_0 = 0.5$) across the (g, λ)-plane as seen in Fig. 10(d) when $m_0 = 1.5$.

5. Summary and Conclusion

We have provided a detailed but succinct review of the VR phenomenon [23], which was proposed two decades ago. We cite numerous works exploring and elucidating the mechanism of VR in several different systems, as well as the contributory or inductive roles of diverse system parameters in the occurrence of VR. Practical experimental realisations and applications of VR have also been explored and discussed.

Figure 10. [Color Online] The dependence of the numerically computed response amplitude Q on the strength of mass nonlinearity λ and the HF signal amplitude g for four values mass amplitude: $m_0 = 0.5$, $m_0 = 1$, $m_0 = 1.3$, $m_0 = 1.5$ shown in (a)–(d), respectively. Other parameters are set as: $\Omega = 9.842$, $\omega = 0.5$, $\alpha = 0.2$, $\beta = 1$, $\omega_0^2 = -1$, $f = 0.05$.

We emphasize that many of the above investigations deal with additive driving forces, whereas rather less attention is paid to parametric driving and amplitude-modulated forcing [34, 65–69]. In connection with signal detection, transmission and amplification, parametric driving and amplitude modulated forcing are excellent tools for achieving higher laser modulation bandwidths which are desirable qualities for applications in multigigabit optical fiber transmitters [107] and could be suitable for designing measurement techniques where high-frequency response is required [108]. Thus, exploring high-frequency parametric vibrations could find practical applications in communications systems as well as in the detection and assessment of structural damages in systems with breathing cracks – suggesting a new direction for vibrational resonance investigations.

Complementing all of the previous VR investigations, where systems had constant mass, we have demonstrated VR in a Duffing oscillator whose mass is position dependent. In particular, we considered the PDM-Duffing, with the mass defined as a regular function comprising of mass amplitude m_0 and strength of spatial nonlinearity λ. Based on the generalized Duffing oscillator equation with PDM, we presented and validated the VR phenomenon in a bistable potential by considering the reduced case in which $m_0 = 1$, $\lambda = 0$. We then extended the problem by examining the effects of the mass parameters on the response curves (Q vs. g) and explored the resonances induced by the PDM parameters in the presence of the HF input signal. We conclude that, in the generalized PDM-Duffing oscillator, the roles played by PDM are both inductive and contributory. They can with advantage be explored to maximize the efficiency of devices that operate in VR modes. We believe that our new formalism describing VR in PDM systems, and its applications as enumerated above, paves the way to a new body of research on vibrational resonance.

Data Accessibility.   No additional supporting data accompanied the submission.

Authors' Contributions.   **TOR**: Methodology, Investigation, Software, Analysis, Writing - Original Draft, **UEV**: Conceptualization, Methodology, Investigation, Software, Analysis, Resources, Project administration, Supervision, Writing - Original Draft, Writing- Reviewing and Editing, **SAA**: Methodology, Investigation, Software, Analysis, **OOP**: Project administration, Supervision, Writing- Reviewing and Editing, **JAL**:

References

1. Strogatz S H. 1994 *Nonlinear Dynamics and Chaos with Applications in Physics, Biology, Chemistry and Engineering*, Reading, Massacusetts: Perseus Book Publishing.
2. Fidlin A. 2006 *Nonlinear Oscillations in Mechanical Engineering*, Berlin, Heidelberg: Springer-Verlag.
3. Irschik H, Belyaev A K, eds. 2014 *Dynamics of Mechanical Systems with Variable Mass*, vol. 557 of *CISM International Centre for Mechanical Sciences*, Germany: Springer-Verlag Wien, 1 edn.
4. Cveticanin L. 2016 *Dynamics of Bodies with Time-Variable Mass*, Mathematical and Analytical Techniques with Applications to Engineering, Switzerland: Springer International Publishing, 1 edn.
5. Awrejcewicz J. 2012 Dynamics of systems of variable mass, in *Classical Mechanics*, pp. 341–357, Springer.
6. Pesce C P, Casetta L. 2014 Systems with mass explicitly dependent on position, in *Dynamics of Mechanical Systems with Variable Mass*, chap. 3, pp. 51–106, Vienna: Springer Vienna.
7. Aquino N, Campoy G, Yee-Madeira H. 1998 The inversion potential for NH_3 using a DFT approach. *Chem. Phys. Lett.* **296**, 111 – 116.
8. Pratim Ghosh A, Mandal A, Sarkar S, Ghosh M. 2016 Influence of position-dependent effective mass on the nonlinear optical properties of impurity doped quantum dots in presence of Gaussian white noise. *Opt. Commun.* **367**, 325 – 334.
9. Zhao Q, *et al.* 2020 Influence of position-dependent effective mass on the nonlinear optical properties in $Al_xGa_{1-x}As/GaAs$ single and double triangular quantum wells. *Physica E* **115**, 113707.
10. Krane K S. 1981 The falling raindrop: variations on a theme of Newton. *Amer. J. Phys.* **49**, 113–117.
11. Bate M R. 2000 Predicting the properties of binary stellar systems: the evolution of accreting protobinary systems. *Mon. Not. R. Astron. Soc.* **314**, 33–53.
12. Burov S, Gitterman M. 2016 Noisy oscillator: Random mass and random damping. *Phys. Rev. E* **94**, 052144.
13. Gammaitoni L, Hänggi P, Jung P, Marchesoni F. 1998 Stochastic resonance. *Rev. Mod. Phys.* **70**, 223–287.
14. Mathews P M, Lakshmanan M. 1974 On a unique nonlinear oscillator. *Quart. Appl. Math.* **32**, 215–218.
15. Bravo R, Plyushchay M S. 2016 Position-dependent mass, finite-gap systems, and supersymmetry. *Phys. Rev. D* **93**, 105023.
16. da Costa B G, Gomez I. 2020 Information-theoretic measures for a position-dependent mass system in an infinite potential well. *Physica A* **541**, 123698.
17. Venkatesan A, Lakshmanan M. 1997 Nonlinear dynamics of damped and driven velocity-dependent systems. *Phys. Rev. E* **55**, 5134–5146.
18. Bagchi B, Das S, Ghosh S, Poria S. 2012 Nonlinear dynamics of a position-dependent mass-driven Duffing-type oscillator. *J. Phys. A: Math. Theor.* **46**, 032001.
19. Mustafa O. 2013 Comment on nonlinear dynamics of a position-dependent mass-driven Duffing-type oscillator. *J. Phys. A: Math. Theor.* **46**, 368001.
20. Cruz S C Y, Rosas-Ortiz O. 2013 Dynamical equations, invariants and spectrum generating algebras of mechanical systems with position-dependent mass. *Symmetry Integr. Geom.* **9**, 4–21.
21. Rajasekar S, Sanjuán M A F. 2016 *Nonlinear Resonances,* Springer Series in Synergetics, Switzerland: Springer.

22. Stocks N G, Stein N D, Soskin S M, McClintock P V E. 1992 Zero-dispersion stochastic resonance. *J. Phys. A: Math. and Gen.* **25**, L1119–L1125.
23. Landa P S, McClintock P V E. 2000 Vibrational resonance. *J. Phys. A: Math. Gen.* **33**, L433–L438.
24. Gitterman M. 2001 Bistable oscillator driven by two periodic fields. *J. Phys. A: Math. Gen.* **34**, L355–357.
25. Gandhimathi V M, Rajasekar S, Kurths J. 2006 Vibrational and stochastic resonances in two coupled overdamped anharmonic oscillators. *Phys. Lett. A* **360**, 279–286.
26. Dykman M I, Luchinsky D G, Mannella R, McClintock P V E, Stein N D, Stocks N G. 1995 Stochastic resonance in perspective. *Nuovo Cimento D* **17**, 661–683.
27. Dykman M I, McClintock P V E. 1998 What can stochastic resonance do? *Nature* **391**, 344.
28. Baltanás J P, *et al.* 2003 Experimental evidence, numerics, and theory of vibrational resonance in bistable systems. *Phys. Rev. E* **67**, 066119.
29. Chizhevsky V N, Giacomelli G. 2006 Experimental and theoretical study of vibrational resonance in a bistable system with asymmetry. *Phys. Rev. E* **73**, 022103.
30. Chizhevsky V N. 2008 Analytical study of vibrational resonance in an overdamped bistable oscillator. *Intern. J. Bifurc. Chaos* **18**, 1767–1773.
31. Chizhevsky V N. 2014 Vibrational higher-order resonances in an overdamped bistable system with biharmonic excitation. *Phys. Rev. E* **90**, 042924.
32. Yang J H, Sanjuán M A F, Tian F, Yang H F. 2015 Saddle-node bifurcation and vibrational resonance in a fractional system with an asymmetric bistable potential. *Intern. J. Bifurc. Chaos* **25**, 1550023.
33. Abusoua A, Daqaq M F. 2018 Experimental evidence of vibrational resonance in a mechanical bistable twin-well oscillator. *J. Comput. Nonlinear Dynam.* **13**, 061002.
34. Roy, Somnath, Das, Debapriya, Banerjee, Dhruba. 2020 Nonlinear response of a parametric bistable oscillator with multiple excitations. *Eur. Phys. J. B* **93**, 12.
35. Rajasekar S, Jeyakumari S, Chinnathambi V, Sanjuan M A F. 2010 Role of depth and location of minima of a double-well potential on vibrational resonance. *J. Phys. A: Math. Theor.* **43**, 465101.
36. Rajasekar S, Abirami K, Sanjuán M A F. 2011 Novel vibrational resonance in multistable systems. *Chaos* **21**, 033106.
37. Roy-Layinde T O, Laoye J A, Popoola O O, Vincent U E, McClintock P V E. 2017 Vibrational resonance in an inhomogeneous medium with periodic dissipation. *Phys. Rev. E* **96**, 032209.
38. Du L C, Song W H, Guo W, Mei D C. 2016 Multiple current reversals and giant vibrational resonance in a high-frequency modulated periodic device. *Europhys. Lett.* **115**, 40008.
39. Deng B, Wang J, Wei X, Yu H, Li H. 2014 Theoretical analysis of vibrational resonance in a neuron model near a bifurcation point. *Phys. Rev. E* **89**, 062916.
40. Jeyakumari S, Chinnathambi V, Rajasekar S, Sanjuán M A F. 2009 Analysis of vibrational resonance in a quintic oscillator. *Chaos* **19**, 043128.
41. Jeyakumari S, Chinnathambi V, Rajasekar S, Sanjuán M A F. 2009 Single and multiple vibrational resonance in a quintic oscillator with monostable potentials. *Phys. Rev. E* **80**, 046608.
42. Djomo Mbong T L M, Siewe M S, Tchawoua C. 2016 The effect of the fractional derivative order on vibrational resonance in a special fractional quintic oscillator. *Mech. Res. Commun.* **78**, 13–19.
43. Yan Z, Wang W, Liu X. 2018 Analysis of a quintic system with fractional damping in the presence of vibrational resonance. *Appl. Math. & Comput.* **321**, 780 – 793.
44. Guo W, Ning L. 2020 Vibrational resonance in a fractional order quintic oscillator system with time delay feedback. *Intern. J. Bifurc. Chaos* **30**, 2050025.
45. Deng B, Wang J, Wei X. 2009 Effect of chemical synapse on vibrational resonance in coupled neurons. *Chaos* **19**, 013117.
46. Jeevarathinam C, Rajasekar S, Sanjuán M A F. 2013 Effect of multiple time-delay on vibrational resonance. *Chaos* **23**, 013136.
47. Sakar P, Shankar Ray D. 2019 Vibrational antiresonance in nonlinear coupled systems. *Phys. Rev. E* **99**, 052221.
48. Daza A, Wagemakers A, Rajasekar S, Sanjuán M A F. 2013 Vibrational resonance in a time-delayed genetic toggle switch. *Commun. Nonlinear Sci.* **18**, 411–416.
49. Ning L, Chen Z. 2020 Vibrational resonance analysis in a gene transcriptional regulatory system with two different forms of time-delays. *Physica D* **401**, 132164.

50. Wang C, Yang K, Qu S X. 2014 Vibrational resonance in a discrete neuronal model with time delay. *Int. J. Mod. Phys. B* **28**, 1450103.
51. Hu D L, Liu X B. 2014 Delay-enhanced signal transmission in a coupled excitable system. *Neurocomputing* **135**, 268–272.
52. Yang J H, Liu X B. 2011 Delay-improved signal propagation in globally coupled bistable systems. *Physica Scripta* **83**, 065008.
53. Jeyakumari S, Chinnathambi V, Rajasekar S, Sanjuán M A F. 2011 Vibrational resonance in an asymmetric Duffing oscillator. *Intern. J. Bifurc. Chaos* **21**, 275–286.
54. Yang J, Huang D, Sanjuán M A F, Liu H. 2018 Vibrational resonance in an overdamped system with a fractional order potential nonlinearity. *Intern. J. Bifurc. Chaos* **28**, 1850082.
55. Uzuntarla M, Yılmaz E, Wagemaker A, Ozer M. 2015 Vibrational resonance in a heterogeneous scale free network of neurons. *Commun. Nonlin. Sci. Numer. Simulat.* **22**, 367–374.
56. Deng B, Wang J, Wei X, Tsang K M, Chan W L. 2010 Vibrational resonance in neuron populations. *Chaos* **20**, 013113.
57. Wu X, Yao C, Shuai J. 2015 Enhanced multiple vibrational resonances by Na^+ and K^+ dynamics in a neuron model. *Sci. Rep.* **5**, 7684.
58. Yao C, Ma J, He Z, Qian Y, Liu L. 2019 Transmission and detection of biharmonic envelope signal in a feed-forward multilayer neural network. *Physica A* **523**, 797–806.
59. Han C, *et al.* 2019 Vibrational resonance without tuning in a neuronal parallel array. *Physica A* **523**, 204–210.
60. Yao C, He Z, Nakano T, Qian Y, Shuai J. 2019 Inhibitory-autapse-enhanced signal transmission in neural networks. *Nonlinear Dyn.* **97**, 1425–1437.
61. Ge M, Lu L, Xu Y, Mamatimin R, Pei Q, Jia Y. 2020 Vibrational mono-/bi-resonance and wave propagation in FitzHugh-Nagumo neural systems under electromagnetic induction. *Chaos Solitons Fractals* **133**, 109645.
62. Qin Y, Han C, Che Y, Zhao J. 2018 Vibrational resonance in a randomly connected neural network. *Cogn. Neurodynamics* **12**, 509—-518.
63. Shi J, Huang C, Dong T, Zhang X. 2010 High-frequency and low-frequency effects on vibrational resonance in a synthetic gene network. *Phys. Biol.* **7**, 036006.
64. Baysal V, Yilmaz E. 2020 Effects of electromagnetic induction on vibrational resonance in single neurons and neuronal networks. *Physica A* **537**, 122733.
65. Ghosh S, Ray D S. 2015 Optical Bloch equations in a bichromatic field; vibrational resonance. *Eur. Phys. J. B* **88**, 1434–6036.
66. Yang J, Sanjuán M, Liu H. 2015 Bifurcation and resonance in a fractional Mathieu-Duffing oscillator. *Eur. Phys. J. B* **88**, 310.
67. Djomo Mbong T L M, Siewe Siewe M, Tchawoua C. 2018 Controllable parametric excitation effect on linear and nonlinear vibrational resonances in the dynamics of a buckled beam. *Commun. Nonlinear Sci.* **54**, 377–388.
68. Jia P, Yang H Jand Liu, Hu E. 2018 Improving amplitude-modulated signals by re-scaled and twice sampling vibrational resonance methods. *Pramana - J. Phys.* **91**, 38.
69. Sarkar P, Paul S, Shankar Ray D. 2019 Controlling subharmonic generation by vibrational and stochastic resonance in a bistable system. *J. Stat. Mech.* **2019**, 063211.
70. Djomo-Mbong T L M, Siewe-Siewe M, Tchawoua C. 2015 The effect of nonlinear damping on vibrational resonance and chaotic behavior of a beam fixed at its two ends and prestressed. *Commun. Nonlin. Sci.* **22**, 228–243.
71. Roy-Layinde T O, Laoye J A, Popoola O O, Vincent U E. 2016 Analysis of vibrational resonance in bi-harmonically driven plasma. *Chaos* **26**, 093117.
72. Laoye J A, Roy-Layinde T O, Omoteso K A, Popoola O O, Vincent U E. 2019 Vibrational resonance in a higher-order nonlinear damped oscillator with rough potential. *Pramana - J. Phys.* **93**, 102.
73. Vincent U E, Roy-Layinde T O, Adesina P O, Popoola O O, McClintock P V E. 2018 Vibrational resonance in an oscillator with an asymmetrical deformable potential. *Phys. Rev. E* **98**, 062203.
74. Gosak M, Perc M, Kralj S. 2012 The impact of static disorder on vibrational resonance in a ferroelectric liquid crystal. *Mol. Cryst. Liq. Cryst.* **553**, 13–20.
75. Abirami K, Rajasekar S, Sanjuán M A F. 2013 Vibrational resonance in the Morse oscillator. *Pramana* **81**, 127–141.

76. Olusola O I, Shomotun O P, Vincent U E, McClintock P V E. 2020 Quantum vibrational resonance in a dual-frequency driven Tietz-Hua quantum well. *Phys. Rev. E* **101**, 052216.
77. Abirami K, Rajasekar S, Sanjuán M A F. 2017 Vibrational resonance in a harmonically trapped potential system. *Commun. Nonlinear Sci.* **47**, 370–378.
78. Chizhevsky V N, Smeu E, Giacomelli G. 2003 Experimental evidence of vibrational resonance in an optical system. *Phys. Rev. Lett.* **91**, 220602.
79. Chizhevsky V N. 2015 Noise-induced suppression of nonlinear distortions in a bistable system with biharmonic excitation in vibrational resonance. *Phys. Rev. E* **92**, 032902.
80. Chizhevsky V N. 2014 Experimental evidence of vibrational resonance in a multistable system. *Phys. Rev. E* **89**, 062914.
81. Ren Y, Duan F. 2016 Theoretical and experimental implementation of vibrational resonance in an array of hard limiters. *Physica A* **456**, 319 – 326.
82. Jothimurugan R, Thamilmaran K, Rajasekar S, Sanjuán M A F. 2013 Experimental evidence for vibrational resonance and enhanced signal transmission in Chua's circuit. *Intern. J. Bifurc. Chaos* **23**, 1350189.
83. Venkatesh P R, Venkatesan A. 2016 Vibrational resonance and implementation of dynamic logic gate in a piecewise-linear Murali–Lakshmanan–Chua circuit. *Commun. Nonlinear Sci.* **39**, 271–282.
84. Morfu S, Bordet M. 2018 On the correlation between phase-locking modes and vibrational resonance in a neuronal model. *Commun. Nonlinear Sci.* **55**, 277 – 286.
85. Rajamani S, Rajasekar S, Sanjuán M A F. 2014 Ghost-vibrational resonance. *Commun. Nonlinear Sci.* **19**, 4003–4012.
86. Yang J, Sanjuán M A, Liu H. 2016 Vibrational subharmonic and superharmonic resonances. *Commun. Nonlinear Sci.* **30**, 362–372.
87. Ghosh S, Ray D S. 2013 Nonlinear vibrational resonance. *Phys. Rev. E* **88**, 042904.
88. Jia P X, Wu C J, Yang J H, Sanjuán M A F, Liu G X. 2018 Improving the weak aperiodic signal by three kinds of vibrational resonance. *Nonlinear Dyn* **91**, 2699–2713.
89. Jia P, Yang J, Zhang X, Sanjuán M A F. 2019 On the LFM signal improvement by piecewise vibrational resonance using a new spectral amplification factor. *IET Signal Process.* **13**, 65–69.
90. Coccolo M, Litak G, Seoane J M, Sanjuán M A F. 2015 Optimizing the electrical power in an energy harvesting system. *Intern. J. Bifurc. Chaos* **25**, 1550171.
91. Ren Y, Pan Y, Duan F. 2018 Generalized energy detector for weak random signals via vibrational resonance. *Phys. Lett. A* **382**, 806 – 810.
92. Liu H G, Liu X L, Yang J H, Sanjuán M A F, Cheng G. 2017 Detecting the weak high-frequency character signal by vibrational resonance in the Duffing oscillator. *Nonlinear Dyn* **89**, 2621–2628.
93. Jia P, Yang J, Leng Y. 2020 The echo chirp signal amplification by the vibrational information fusion method. *Int. J. Mod. Phy. B* **34**, 2050041.
94. Liu Y, Dai Z, Lu S, Liu F, Zhao J, Shen J. 2017 Enhanced bearing fault detection using step-varying vibrational resonance based on Duffing oscillator nonlinear system. *Shock Vib.* **2017**, 5716296.
95. Yang J H, Sanjuán M A F, Liu H G. 2017 Enhancing the weak signal with arbitrary high-frequency by vibrational resonance in fractional-order Duffing oscillators. *J. Comput. Nonlinear Dynam.* **12**, 051011.
96. Gao J, Yang J, Huang D, Liu H, Liu S. 2019 Experimental application of vibrational resonance on bearing fault diagnosis. *J Braz. Soc. Mech. Sci. Eng.* **41**, 6(1–13).
97. Xiao L, Zhang X, Lu S, Xia T, Xi L. 2019 A novel weak-fault detection technique for rolling element bearing based on vibrational resonance. *J. Sound Vib.* **438**, 490–505.
98. Venkatesh P R, Venkatesan A, Lakshmanan M. 2017 Implementation of dynamic dual input multiple output logic gate via resonance in globally coupled Duffing oscillators. *Chaos* **27**, 083106.
99. Gui R, Zhang H, Cheng G, Yao Y. 2020 Set–reset latch logic operation in a bistable system under suprathreshold and subthreshold signals. *Chaos* **30**, 023119.
100. Gui R, Wang Y, Yao Y, Cheng G. 2020 Enhanced logical vibrational resonance in a two-well potential system. *Chaos Solitons Fractals* **138**, 109952.
101. Usama B I, Morfu S, Marquié P. 2019 Numerical analyses of the vibrational resonance occurrence in a nonlinear dissipative system. *Chaos, Solitons, Fractals* **127**, 31–37.
102. Cruz y Cruz S, Negro J, Nieto L M. 2007 Classical and quantum position-dependent mass harmonic oscillators. *Phys. Lett. A* **369**, 400 – 406.

103. Mustafa O. 2020 PDM creation and annihilation operators of the harmonic oscillators and the emergence of an alternative PDM-Hamiltonian. *Phys. Lett. A* **384**, 126265.
104. Zhang Y, Li S. 2017 Combination and simultaneous resonances of gas bubbles oscillating in liquids under dual-frequency acoustic excitation. *Ultrason. Sonochem.* **35**, 431–439.
105. Hegedüs F, Klapcsik K, Lauterborn W, Parlitz U, Mettin R. 2020 GPU accelerated study of a dual-frequency driven single bubble in a 6-dimensional parameter space: The active cavitation threshold. *Ultrason. Sonochem.* **67**, 105067.
106. Blekhman I I, Landa P S. 2004 Conjugate resonances and bifurcations in nonlinear systems under biharmonical excitation. *Intern. J. Nonlin. Mech.* **39**, 421–426.
107. Bennett S, Snowden V M, Iezekiel S. 1997 Nonlinear dynamics in directly modulated multiple-quantum-well laser diodes. *IEEE J. Quan. Elect.* **33**, 2076–2083.
108. Lin R M, Ng T Y. 2018 Applications of higher-order frequency response functions to the detection and damage assessment of general structural systems with breathing cracks. *Int. J. Mech. Sci.* **148**, 652–666.